Vol 448 | 16 August 2007 | doi:10.1038/nature06064

LETTERS

Talc-bearing serpentinite and the creeping section of the San Andreas fault

Diane E. Moore[1] & Michael J. Rymer[1]

The section of the San Andreas fault located between Cholame Valley and San Juan Bautista in central California creeps at a rate as high as 28 mm yr^{-1} (ref. 1), and it is also the segment that yields the best evidence for being a weak fault embedded in a strong crust[2–5]. Serpentinized ultramafic rocks have been associated with creeping faults in central and northern California[6–8], and serpentinite is commonly invoked as the cause of the creep and the low strength of this section of the San Andreas fault. However, the frictional strengths of serpentine minerals are too high to satisfy the limitations on fault strength, and these minerals also have the potential for unstable slip under some conditions[9,10]. Here we report the discovery of talc in cuttings of serpentinite collected from the probable active trace of the San Andreas fault that was intersected during drilling of the San Andreas Fault Observatory at Depth (SAFOD) main hole in 2005. We infer that the talc is forming as a result of the reaction of serpentine minerals with silica-saturated hydrothermal fluids that migrate up the fault zone, and the talc commonly occurs in sheared serpentinite. This discovery is significant, as the frictional strength of talc at elevated temperatures is sufficiently low to meet the constraints on the shear strength of the fault, and its inherently stable sliding behaviour is consistent with fault creep[11]. Talc may therefore provide the connection between serpentinite and creep in the San Andreas fault, if shear at depth can become localized along a talc-rich principal-slip surface within serpentinite entrained in the fault zone.

The SAFOD drillsite is located 14 km northwest of Parkfield in central California (Fig. 1), along the creeping section of the San Andreas fault (SAF). In 2005, drilling successfully crossed the active trace of the SAF at ~3 km vertical depth[12], where the measured temperature is ~112 °C (ref. 13). The drillhole terminated in sedimentary rocks of the Great Valley Sequence (K. McDougall, personal communication) east of the fault. Since then, a portion of the well casing has been actively deforming in response to creep on a fault strand[12]. Serpentine was identified in X-ray diffraction patterns of cuttings[14] collected at the eastern margin of the zone of active deformation (Supplementary Fig. 1). Aeromagnetic surveys[15] indicate the presence of a flat-lying slab of serpentinite at >3 km depth on the northeast side of the fault (Fig. 1). This body may be ≥2 km thick, and it abuts the fault for 50–60 km (ref. 15). The serpentinite slab is probably part of the Coast Range ophiolite, the oceanic basement on which the sediments of the Great Valley Sequence were deposited. Serpentinized ultramafic rock has a relatively low density compared to the overlying rock column, and a fault intersecting such a rock unit provides the pathway for the migration of serpentinite to shallower depths[16]. The Table Mountain serpentinite[17] east of Parkfield (Fig. 1) is an extrusive body that formed as a result of the diapiric rise of low-density serpentinite from the deeply buried slab along faults that served as 'fissure feeders'[17]. The serpentinite associated with the active trace in the SAFOD drillhole[14] and outcrops of serpentinite[18,19] fault gouge (Fig. 1) suggest that the same process is occurring along the SAF.

Serpentinite has been suggested as a possible cause of creep, because of its close association with creeping faults in central and northern California[6–8]. The SAF creeping section coincides with the

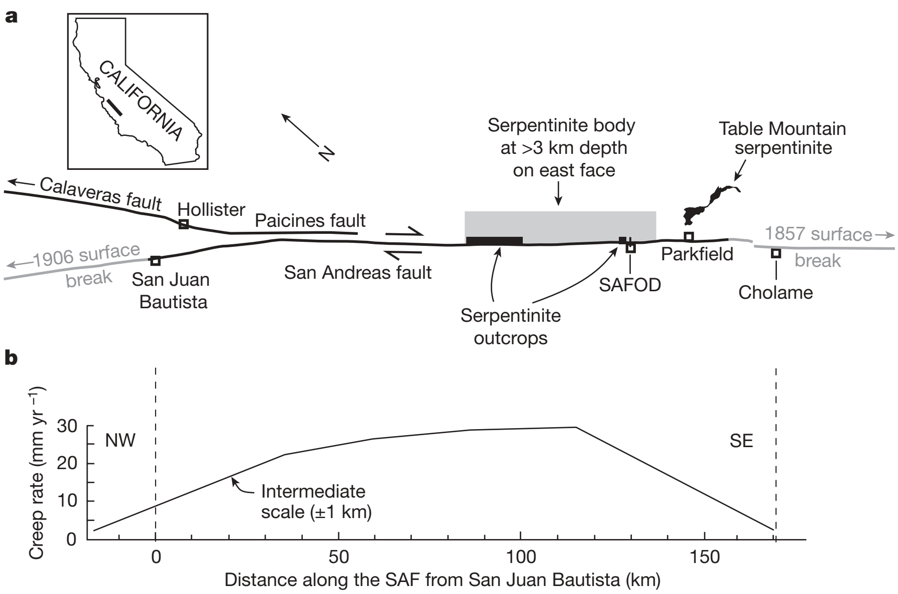

Figure 1 | Distribution of serpentinite along the SAF creeping section. a, The creeping section lies between areas of the fault that ruptured during great earthquakes in 1857 and 1906. Serpentinite occurs in rare surface exposures of the fault[18,19] and in the probable active trace of the fault encountered at ~3 km vertical depth in the SAFOD drillhole[12,14]. The extrusive serpentinite at Table Mountain[17] is derived from the same serpentinite body that abuts the fault on the northeast side at >3 km depth[15]. **b**, Recently updated creep rates measured at distances of 10 m to 1 km from the fault[1]. Total offset rates along the San Andreas system in the creeping section are considered to be between 28 and 34 mm yr^{-1} (ref. 1).

[1]US Geological Survey, 345 Middlefield Road, Mail Stop 977, Menlo Park, California 94025, USA.

mapped extent of Coast Range ophiolite and overlying Great Valley Sequence rocks on the northeast side of the fault[7,8,20]. Ultramafic rocks of the Coast Range ophiolite are variably serpentinized. The most extensive serpentinite body along this section is the one east of SAFOD[15] that is associated with the highest creep rate (Fig. 1). On the basis of aeromagnetic and gravity surveys, a slab of serpentinite 1–1.5 km thick at $\geq$3 km depth extends northeastwards from the SAF a few kilometres southeast of San Juan Bautista to the Calaveras fault around Hollister[20]. Serpentinite continues at somewhat greater depth[20] east of the Calaveras fault in that area. Other, smaller masses of serpentinite are present at $\geq$2.4 km depth between the San Andreas and Paicines faults[7]. The Calaveras–Paicines faults creep at rates of 6–10 mm yr^{-1} south of Hollister[21].

The creeping section provides the best evidence for a weak SAF[2–5]. Because the creeping section is characterized by aseismic slip and microearthquakes, the apparent weakness of this segment cannot be explained through some dynamic weakening process accompanying a major earthquake, as it can for the locked sections. The restrictions on shear strength in the creeping SAF imposed by heat-flow[22,23] and stress-orientation[24,25] data are delimited in Fig. 2; also included are the frictional strengths of synthetic fault-gouge materials[9–11,26] prepared by grinding and sieving rock or mineral separates. The strength experiments were conducted in a triaxial machine fitted with an internal furnace, at various combinations of temperature, confining and fluid pressure, and sliding velocity. For a given mineral to control the behaviour of the creeping section, it must be very weak as well as characterized by stable shear. The frictional properties of the serpentine minerals do not satisfy the weakness criterion and under certain conditions do not satisfy the stability criterion. The serpentine minerals lizardite and antigorite[9] are not substantially weaker than granite[26] under hydrothermal conditions (Fig. 2). Chrysotile satisfies the heat-flow constraint to depths of ~3 km, but its strength increases substantially at greater depths[9,10]. Furthermore, all three serpentine minerals show both velocity-weakening (strength decreases with increasing velocity) and velocity-strengthening (strength increases with increasing velocity) behaviour[9,10] at different temperature–pressure–velocity conditions; as a result, they can slip either unstably or stably, respectively, depending on the depth and slip rate.

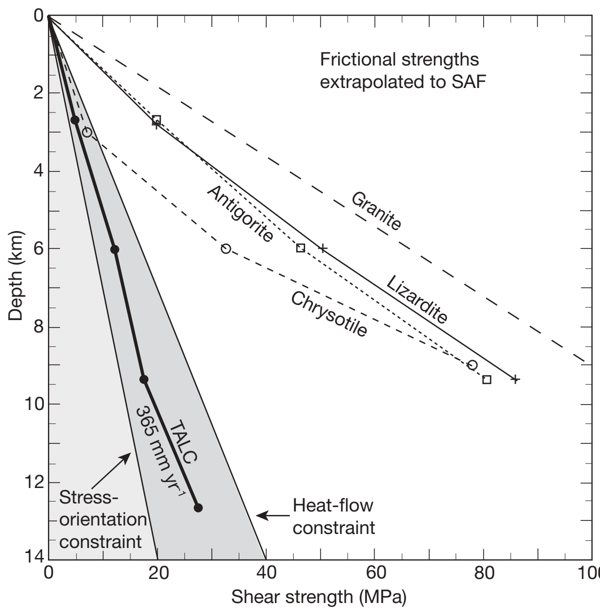

Figure 2 | Shear strength versus fault depth. Shaded fields indicate the constraints on the strength of the SAF based on heat-flow[22,23] and stress-orientation[24,25] investigations. Shear-strength data plotted for granite[26], serpentine minerals[9–11] and talc[11] assume a temperature gradient of 30 °C km^{-1} and a hydrostatic fluid-pressure gradient. At depths $\leq$3 km, both chrysotile and talc satisfy the heat-flow constraint, but chrysotile becomes substantially stronger at greater depths. The talc data represent a sliding velocity of 365 mm yr^{-1}. Given the characteristic velocity-strengthening behaviour of talc[11], its shear strength at $\leq$30 mm yr^{-1} (Fig. 1) may be even lower.

We examined serpentinite grains from the washed SAFOD cuttings that were collected at ~3 m intervals during drilling. Polished grain mounts were prepared from cuttings samples for analysis with an optical microscope, scanning electron microscope (SEM) and electron microprobe. The serpentinite contents of the bulk cuttings, estimated from point counts of thin sections, exceeds 2% by volume in the interval 3,319–3,350 m measured depth (MD), with a spike of ~8% in the 3,325 m MD sample (Supplementary Fig. 1). A powder X-ray diffraction pattern of a separate of serpentinite grains shows prominent peaks consistent with lizardite and chrysotile, the two low-temperature serpentine minerals. No relict olivine or pyroxene has been found. On the basis of the common occurrence of both mesh texture after olivine and bastite texture after pyroxene, the original ultramafic rock was probably a harzburgite[16], similar to the Table Mountain serpentinite[17]. The pseudomorphic mesh and bastite textures have been extensively modified by recrystallization, brecciation and shearing.

The serpentinite contains numerous calcite- and some quartz-filled veins, possibly resulting from focused fluid flow within the fault zone. Talc replaces serpentine minerals along the vein walls (Fig. 3a, b), and it fills narrow cracks that extend into the serpentinite from the wider veins. Talc also forms along the foliation in sheared serpentinite grains (Fig. 3c, d). The talc-forming reaction is:

$$\underset{\text{serpentine}}{Mg_3Si_2O_5(OH)_4} + 2SiO_2 = \underset{\text{talc}}{Mg_3Si_4O_{10}(OH)_2} + H_2O$$

The SiO_2 comes from the dissolved silica content of heated ground water (Fig. 3a, c, d) and from quartz deposited metastably in veins (Fig. 3b). Talc is stable relative to the assemblage quartz + serpentine throughout the stability range of serpentine[27]. The veins and shears with which talc is associated overprint all other textural features in the serpentinite grains, suggesting that the talc is of recent origin. Talc

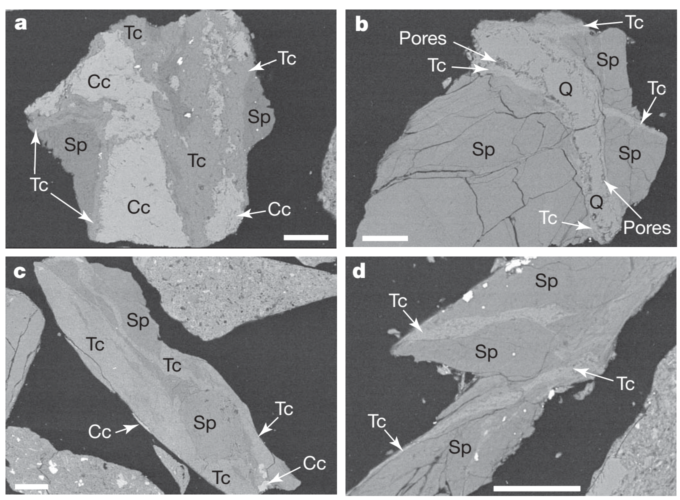

Figure 3 | Talc occurrences in serpentinite grains. Backscattered-electron SEM images of talc-bearing serpentinite grains from cuttings collected at 3,325 m MD. **a**, Talc (Tc) replacing serpentine minerals (Sp) adjacent to vein calcite (Cc). **b**, The reaction of serpentine and vein quartz (Q) to produce talc. The reaction results in a decrease in the volume of solid phases, consistent with the concentration of pores between the talc and quartz. **c**, Talc forming along the foliation in a sheared serpentinite grain. **d**, Talc in sheared serpentinite. Talc commonly appears at the edges of grains, perhaps because the serpentinite preferentially breaks along the weaker talc during drilling. Scale bars, 50 μm.

is most abundant in the 3,325 m MD sample, which also contains nearly all of the sheared talc-bearing grains identified thus far. Talc is only a minor component of the serpentinite ($\leq$2–3%), although this soft mineral may have been preferentially lost during drilling (Fig. 3d).

Talc compositions (Supplementary Table 1) are consistent with those of talc in other low-temperature hydrothermal environments[27]. The talc typically contains 4.0–5.5 wt% FeO and as much as 1.5 wt% NiO. In contrast, talc takes up only minor amounts of Al, and the Mg-rich smectite clay mineral saponite, with ~5.0–7.5 wt% Al_2O_3 (Supplementary Table 1), replaces serpentine that has been mixed with feldspathic sediments.

The presence of talc in the active trace of the SAF is significant because talc has a very low shear strength in the temperature range 100–400 °C (Fig. 2). Talc may be the only mineral that can satisfy the conditions for a weak SAF over the entire depth range of the seismogenic zone without the need to invoke additional weakening mechanisms such as fluid overpressures. It is also characterized by inherently stable, velocity-strengthening behaviour[11]. In rocks of appropriate composition, talc is stable at temperatures ranging from surficial to nearly 800 °C (ref. 27). The frictional strength of water-saturated smectite clay is comparable to that of talc at room temperature[28]. However, the smectite clay saponite begins to break down at temperatures slightly above 100 °C (ref. 29), transforming to chlorite the water-saturated frictional strength of which[28] is close to that of lizardite. As with chrysotile (Fig. 2), saponite cannot explain the low apparent strength of the creeping section at depths greater than 3–4 km.

This discovery reinstates serpentinite as a possible explanation for fault creep, although indirectly through its association with talc; testing this hypothesis may prove challenging. The collection of core from the active trace of the SAF planned for 2007 at SAFOD may provide some answers, although, as noted previously, chrysotile and smectite clays have comparable frictional properties to talc at ~3 km depth. The small amount of talc found in the cuttings raises the question of whether enough talc could be present at greater depths to influence fault behaviour. However, along the Punchbowl fault, an exhumed former strand of the SAF in southern California, offset became extremely localized to a single fracture surface within a narrow (0.15–0.55 m) fault core[30]. For such a fault geometry, only enough talc to line a fracture surface in serpentinite would be needed. Shear of laboratory samples of serpentinite and talc is typically highly localized[9–11] along shear planes similar to the one in the Punchbowl fault. The talc-forming reaction should also be enhanced at depths >3 km, because of faster reaction rates and the ability of higher-temperature ground waters to introduce larger amounts of dissolved silica to the serpentinite.

Received 6 March; accepted 3 July 2007.

1. Titus, S. J., DeMets, C. & Tikoff, B. Thirty-five-year creep rates for the creeping segment of the San Andreas fault and the effects of the 2004 Parkfield earthquake: Constraints from alignment arrays, continuous global positioning system, and creepmeters. *Bull. Seismol. Soc. Am.* **96** (4B), S250–S268 (2006).
2. Provost, A.-S. & Houston, H. Orientation of the stress field surrounding the creeping section of the San Andreas fault: Evidence for a narrow mechanically weak fault zone. *J. Geophys. Res.* **106,** 11373–11386 (2001).
3. Hickman, S. & Zoback, M. Stress orientations and magnitudes in the SAFOD pilot hole. *Geophys. Res. Lett.* **31,** L15S12, doi:10.1029/2004GL020043 (2004).
4. Chéry, J., Zoback, M. D. & Hickman, S. A mechanical model of the San Andreas fault and SAFOD Pilot Hole stress measurements. *Geophys. Res. Lett.* **31,** L15S13, doi:10.1029/2004GL019521 (2004).
5. Williams, C. F., Grubb, F. V. & Galanis, S. P. Jr. Heat flow in the SAFOD pilot hole and implications for the strength of the San Andreas Fault. *Geophys. Res. Lett.* **31,** L15S14, doi:10.1029/2003GL019352 (2004).
6. Allen, C. R. in *Proc. Conf. on Geologic Problems of San Andreas Fault System* (eds Dickinson, W. R. & Grantz, A.) 70–80 (Stanford University Publications in the Geological Sciences Vol. 11, Stanford University, Stanford, California, 1968).
7. Hanna, W. F., Brown, R. D. Jr, Ross, D. C. & Griscom, A. Aeromagnetic reconnaissance and generalized geologic map of the San Andreas fault between San Francisco and San Bernardino, California. *US Geol. Surv. Geophys. Investig. Map GP-815* (1972).
8. Irwin, W. P. & Barnes, I. Effect of geologic structure and metamorphic fluids on seismic behavior of the San Andreas fault system in central and northern California. *Geology* **3,** 713–716 (1975).
9. Moore, D. E., Lockner, D. A., Ma, S., Summers, R. & Byerlee, J. D. Strengths of serpentinite gouges at elevated temperatures. *J. Geophys. Res.* **102,** 14787–14801 (1997).
10. Moore, D. E., Lockner, D. A., Tanaka, H. & Iwata, K. in *Serpentine and Serpentinites: Mineralogy, Petrology, Geochemistry, Ecology, Geophysics, and Tectonics* (ed. Ernst, W.G.) 525–538 (International Book Series Vol. 8, Geological Society of America, Boulder, Colorado, 2004).
11. Moore, D. E. & Lockner, D. A. Comparative deformation behavior of minerals in serpentinized ultramafic rock: Application to the slab-mantle interface in subduction zones. *Int. Geol. Rev.* **49,** 401–415 (2007).
12. Zoback, M. D., Hickman, S. & Ellsworth, W. Overview of SAFOD Phases 1 and 2: Drilling, sampling and measurements of the San Andreas Fault zone at seismogenic depth. *Eos* **86** (Fall Meet. Suppl.), abstr. T23E–01 (2005).
13. Williams, C. F., Grubb, F. V. & Galanis, S. P. Heat-flow measurements across the San Andreas fault near Parkfield, California — Preliminary results from SAFOD. *Eos* **87**(Fall Meet. Suppl.), abstr. S33B–0241 (2006).
14. Solum, J. G. *et al.* Mineralogical characterization of protolith and fault rocks from the SAFOD main hole. *Geophys. Res. Lett.* **33,** L21314, doi:10.1029/2006GL027285 (2006).
15. McPhee, D. K., Jachens, R. C. & Wentworth, C. M. Crustal structure across the San Andreas Fault at the SAFOD site from potential field and geologic studies. *Geophys. Res. Lett.* **31,** L12S03, doi:10.1029/2003GL019363 (2004).
16. Coleman, R. G. Petrologic and geophysical nature of serpentinites. *Geol. Soc. Am. Bull.* **82,** 897–918 (1971).
17. Dickinson, W. R. Table Mountain serpentinite extrusion in California Coast Ranges. *Geol. Soc. Am. Bull.* **77,** 451–472 (1966).
18. Rymer, M. J. Geologic map along a 12 kilometer segment of the San Andreas fault zone, southern Diablo Range, California (scale 1:12,000). *US Geol. Surv. Open-File Rep. 81–1173* (1981).
19. Rymer, M. J. *et al.* Surface fault slip associated with the 2004 Parkfield, California, earthquake. *Bull. Seismol. Soc. Am.* **96** (4B), S11–S27 (2006).
20. Robbins, S. L. Complete Bouguer gravity, aeromagnetic, and generalized geologic map of the Hollister 15-minute quadrangle, California (scale 1:62,500). *US Geol. Surv. Geophys. Investig. Map GP-945* (1982).
21. Galehouse, J. S. & Lienkaemper, J. J. Inferences drawn from two decades of alinement array measurements of creep on faults in the San Francisco Bay region. *Bull. Seismol. Soc. Am.* **93,** 2415–2433 (2003).
22. Brune, J. N., Henyey, T. L. & Roy, R. F. Heat flow, stress and rate of slip along the San Andreas fault, California. *J. Geophys. Res.* **74,** 3821–3827 (1969).
23. Lachenbruch, A. H. & Sass, J. H. Heat flow and energetics of the San Andreas fault zone. *J. Geophys. Res.* **85,** 6185–6223 (1980).
24. Mount, V. S. & Suppe, J. State of stress near the San Andreas fault: Implications for wrench tectonics. *Geology* **15,** 1143–1146 (1987).
25. Zoback, M. D. *et al.* New evidence for the state of stress on the San Andreas fault system. *Science* **238,** 1105–1111 (1987).
26. Blanpied, M. L., Lockner, D. A. & Byerlee, J. D. Frictional slip of granite at hydrothermal conditions. *J. Geophys. Res.* **100,** 13045–13064 (1995).
27. Evans, B. W. & Guggenheim, S. in *Hydrous Phyllosilicates (Exclusive of Micas)* (ed. Bailey, S.W.) 225–294 (Reviews in Mineralogy Vol. 19, Mineralogical Society of America, Washington DC, 1988).
28. Moore, D. E. & Lockner, D. A. Crystallographic controls on the frictional behavior of dry and water-saturated sheet structure minerals. *J. Geophys. Res.* **109,** B03401, doi:10.1029/2003JB002582 (2004).
29. Inoue, A. & Utada, M. Smectite-to-chlorite transformation in thermally metamorphosed volcaniclastic rocks in the Kamikita area, northern Honshu, Japan. *Am. Mineral.* **76,** 628–640 (1991).
30. Chester, F. M. & Chester, J. S. Ultracataclasite structure and friction processes of the Punchbowl fault, San Andreas system, California. *Tectonophysics* **295,** 199–221 (1998).

Supplementary Information is linked to the online version of the paper at www.nature.com/nature.

Author Information Reprints and permissions information is available at www.nature.com/reprints. The authors declare no competing financial interests. Correspondence and requests for materials should be addressed to D.E.M. (dmoore@usgs.gov).